Electronic Supplementary Information

High-efficiency transformation of amorphous carbon into graphite nanoflakes for stable aluminum-ion battery cathodes

Jiguo Tu,[a] Junxiang Wang,[a] Shijie Li,[a] Wei-Li Song,[*,b] Mingyong Wang,[*,a] Shuqiang Jiao[*,a] and Hongmin Zhu [a,c]

[a] State Key Laboratory of Advanced Metallurgy, University of Science and Technology Beijing, Beijing, 100083, PR China

[b] Institute of Advanced Structure Technology, Beijing Institute of Technology, Beijing 100081, PR China

[c] Department of Metallurgy, Graduate School of Engineering, Tohoku University, Sendai, Miyagi 9808579, Japan

***Corresponding Author**

E-mail: weilis@bit.edu.cn, Tel: +86-10-68913302, Fax: +86-10-68913302

E-mail: mywang@ustb.edu.cn, Tel: +86-10-62333617, Fax: +86-10-62333617

E-mail: sjiao@ustb.edu.cn, Tel: +86-10-62333617, Fax: +86-10-62333617

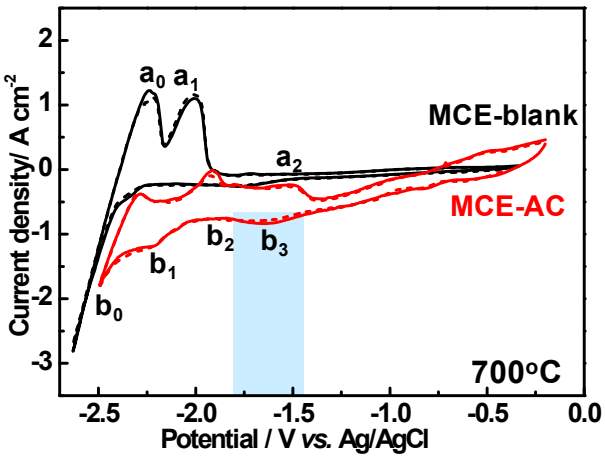

Fig. S1. CV curves of the blank MCE and MCE loaded with amorphous carbon in $CaCl_2$-LiCl melts at 700 °C at a scan rate of 50 mV s^{-1}.

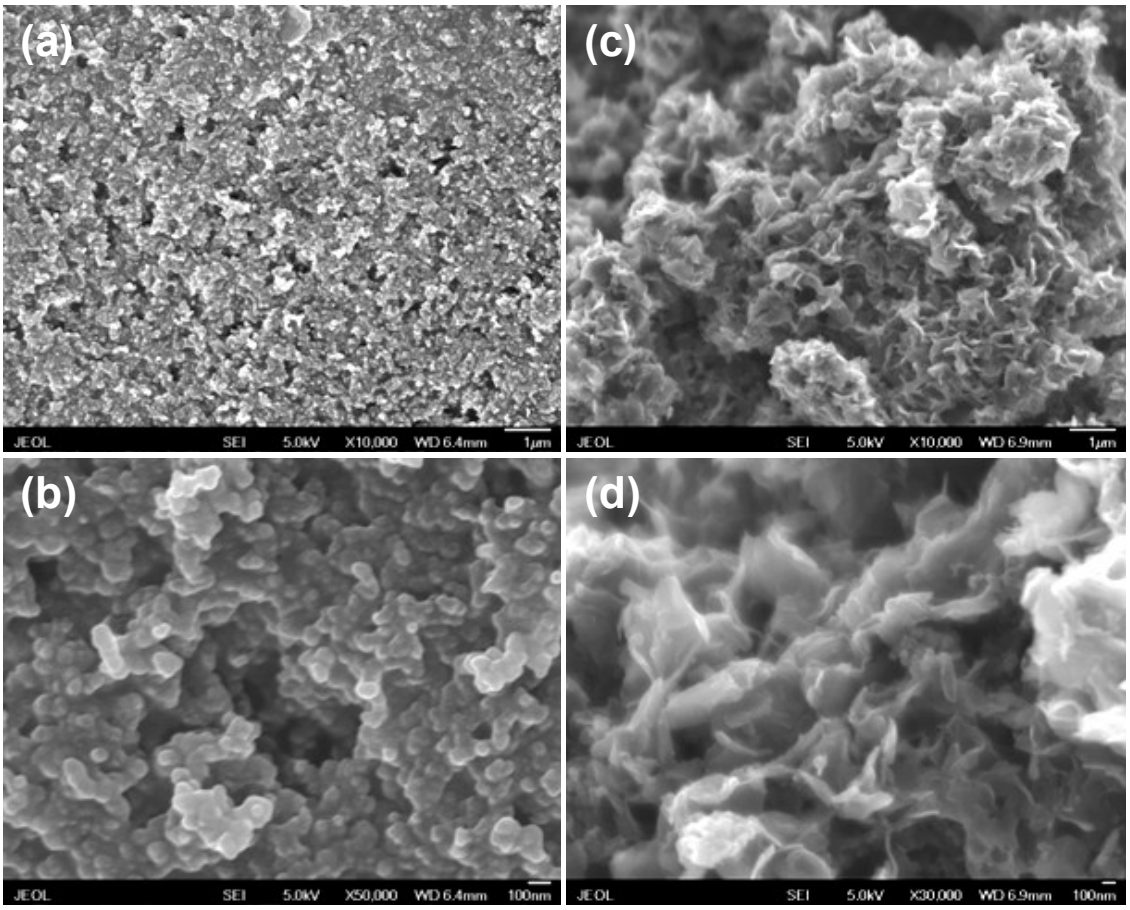

Fig. S2. SEM images of the as-prepared samples through constant cell voltage electrolysis under 3.0 V at 700 °C for 2 h (a,b) and 5 h (c,d).

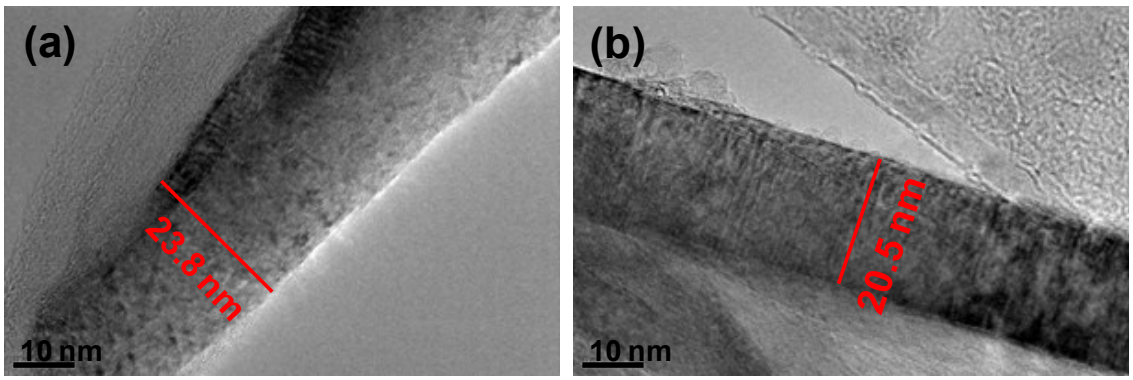

Fig. S3. HRTEM images of amorphous carbon after cathodic electrolysis under different constant cell voltages of 2.8 V (a) and 3.0 V (b) at 800 °C for 2 h.

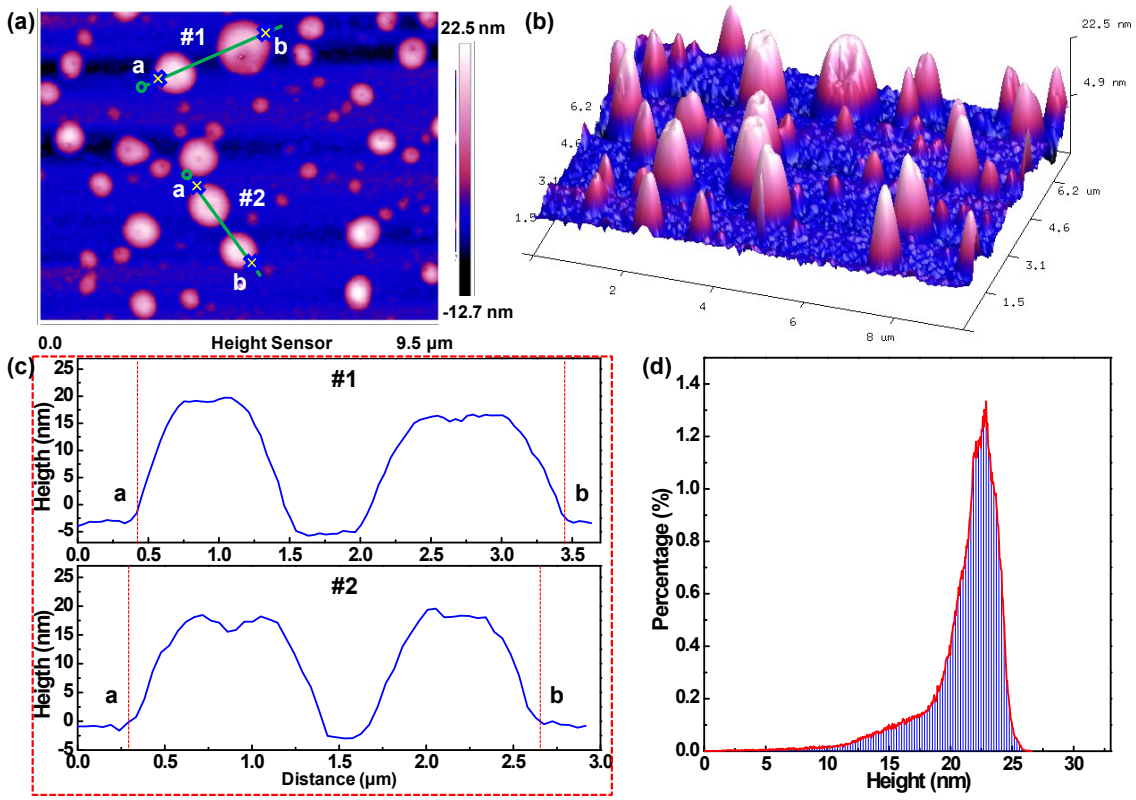

Fig. S4. Typical AFM and 3D AFM images of the electrolyzed sample under 3.0 V at 800 °C for 2 h (a,b). The thinness at different locations (c). Percentage of average thickness distribution of the electrolyzed sample (d).

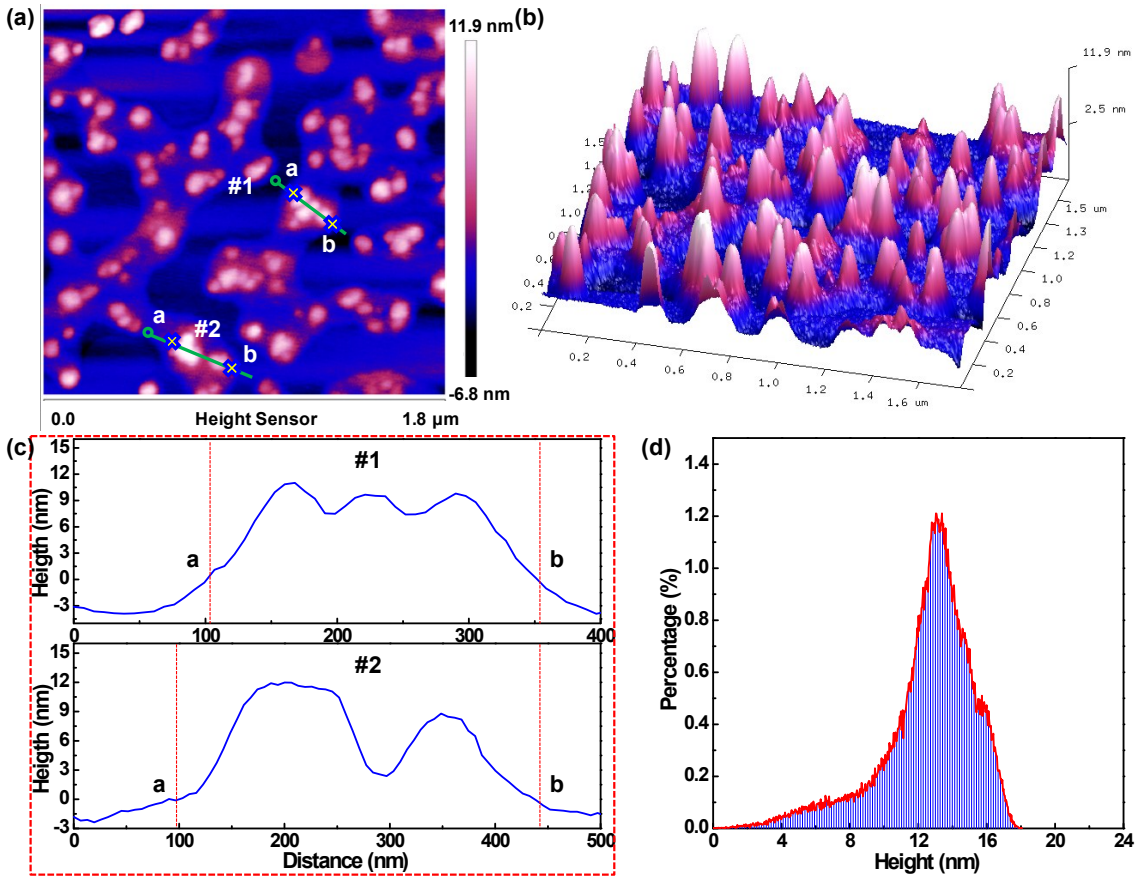

Fig. S5. Typical AFM and 3D AFM images of the electrolyzed sample under 2.8 V at 850 °C for 2 h (a,b). The thinness at different locations (c). Percentage of average thickness distribution of the electrolyzed sample (d).

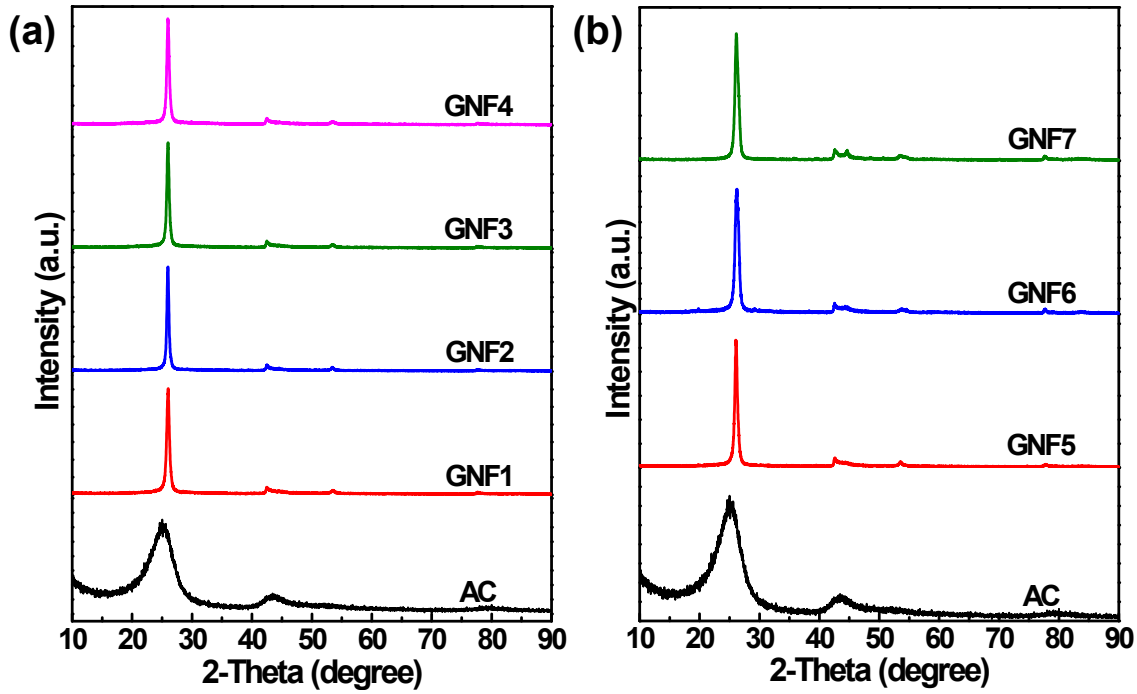

Fig. S6. XRD patterns of amorphous carbon before and after cathodic electrolysis under different constant cell voltages at 800 °C for 2h (a). XRD patterns of amorphous carbon before and after cathodic electrolysis under 2.8 V at 850 °C for different times (b).

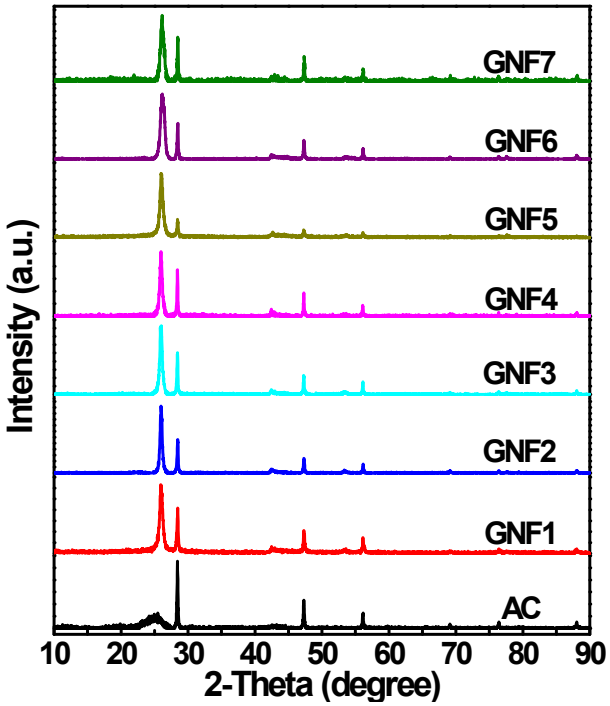

Fig. S7. XRD patterns of amorphous carbon before and after cathodic electrolysis at the indicated conditions with a small number of Si standard powders.

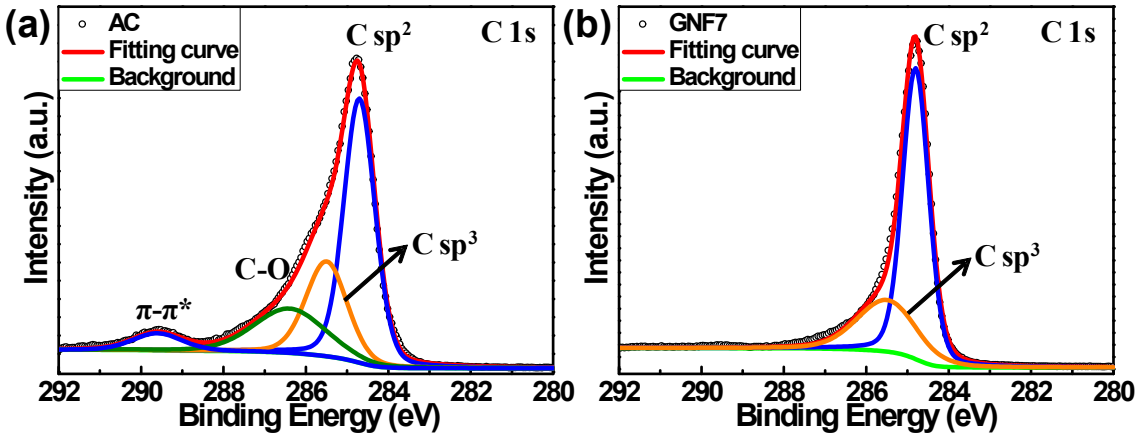

Fig. S8. High-resolution XPS spectra of C1s for AC (a) and GNF7 (b).

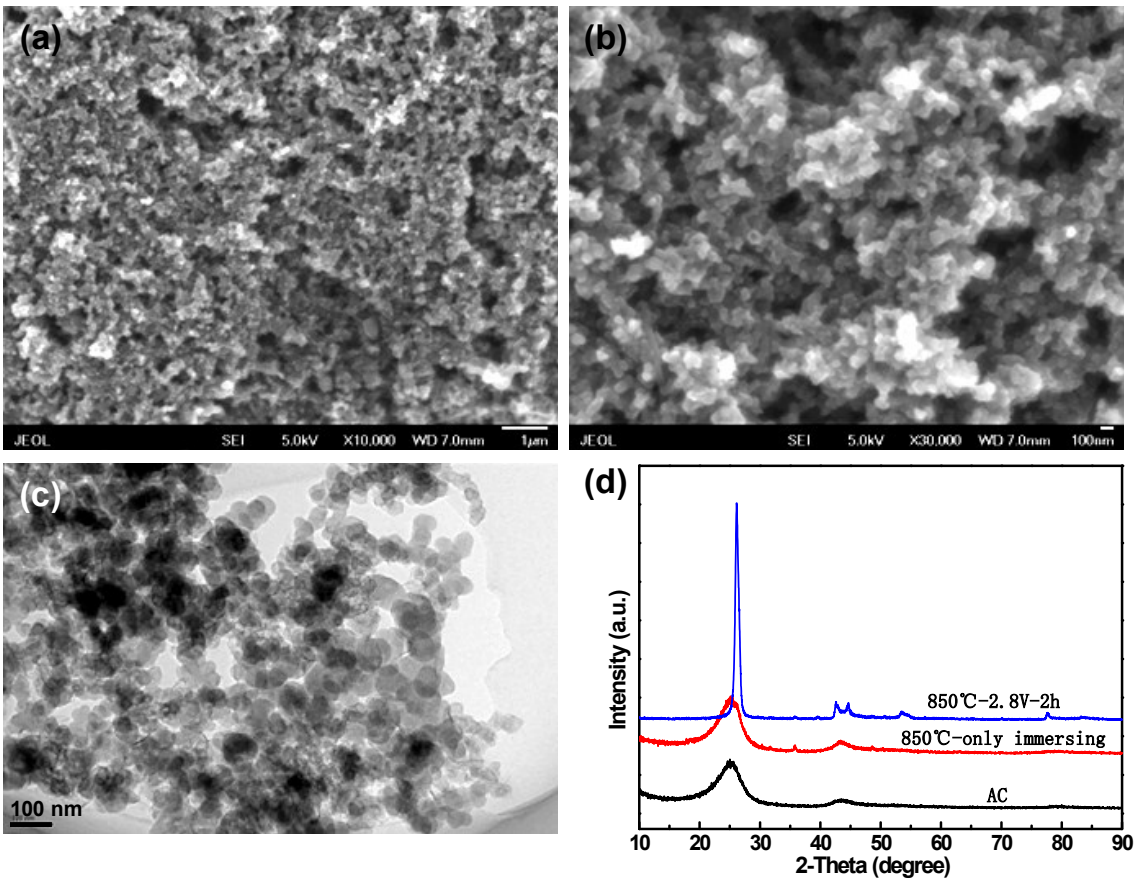

Fig. S9. SEM images (a,b), TEM image (c) and Raman spectra (d) of the as-prepared sample by only immersing amorphous carbon into $CaCl_2$-LiCl salt at 850 °C for 3 h.

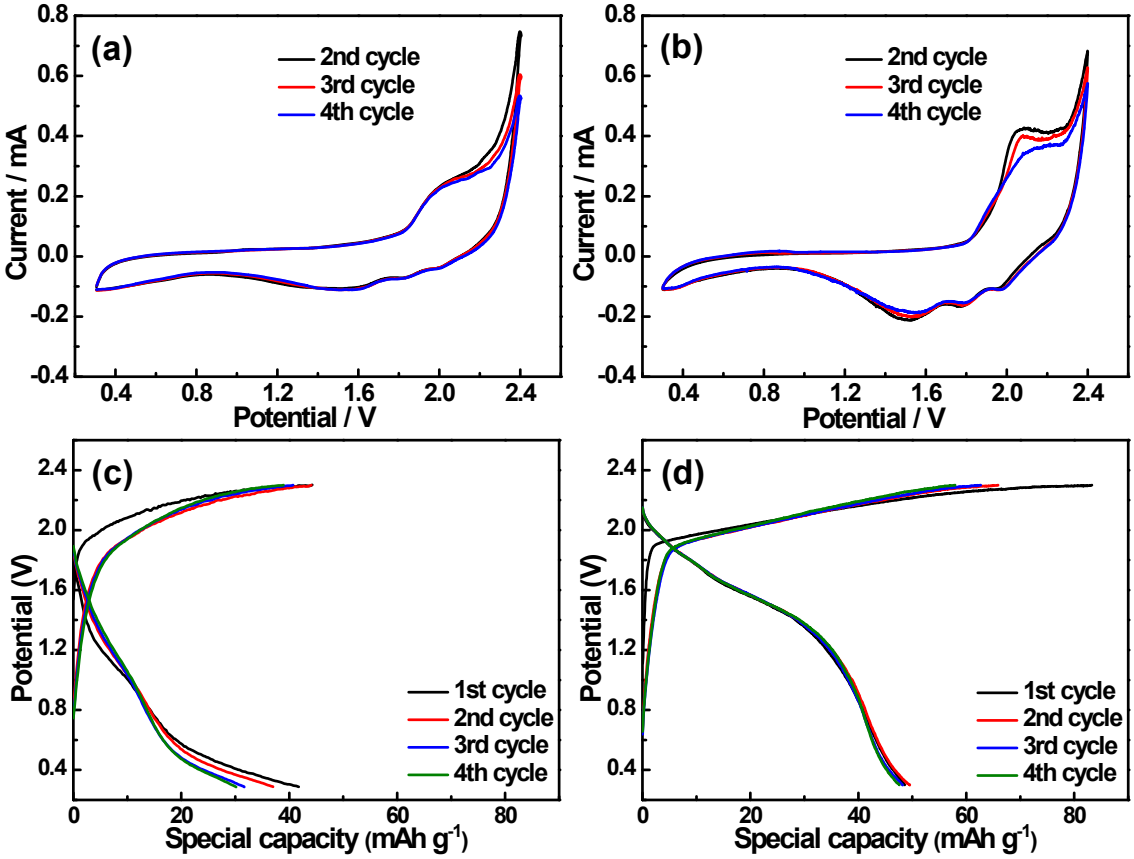

Fig. S10. CV curves of AC (a) and GNF7 (b) from 2n to 4th cycle at a scan rate of 0.5 mV s^{-1}. The charge-discharge curves for the first four cycles of AC (c) and GNF7 (d) at a current density of 100 mA g^{-1} under the potentials ranging from 0.3 to 2.3 V.

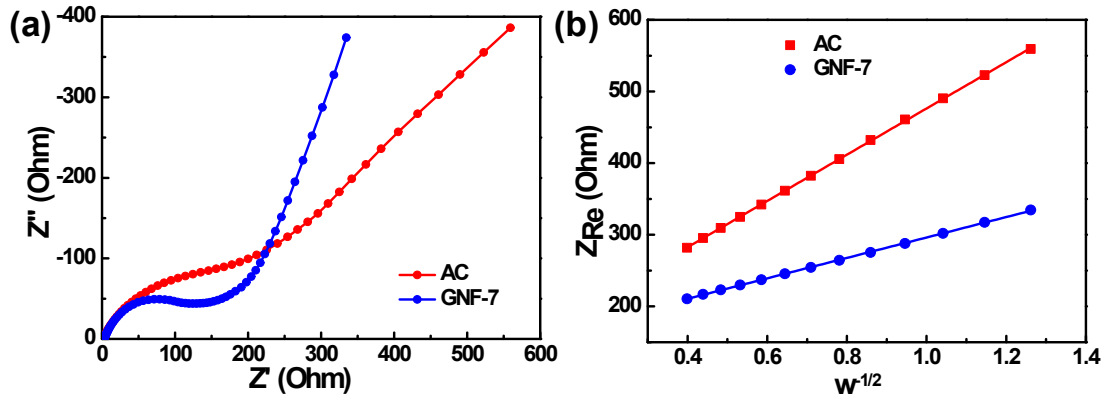

Fig. S11. Nyquist plots (a) and the relationship between Z_{Re} and $\omega^{-1/2}$ (b) of AC and GNF-7 electrodes over 10 cycles.

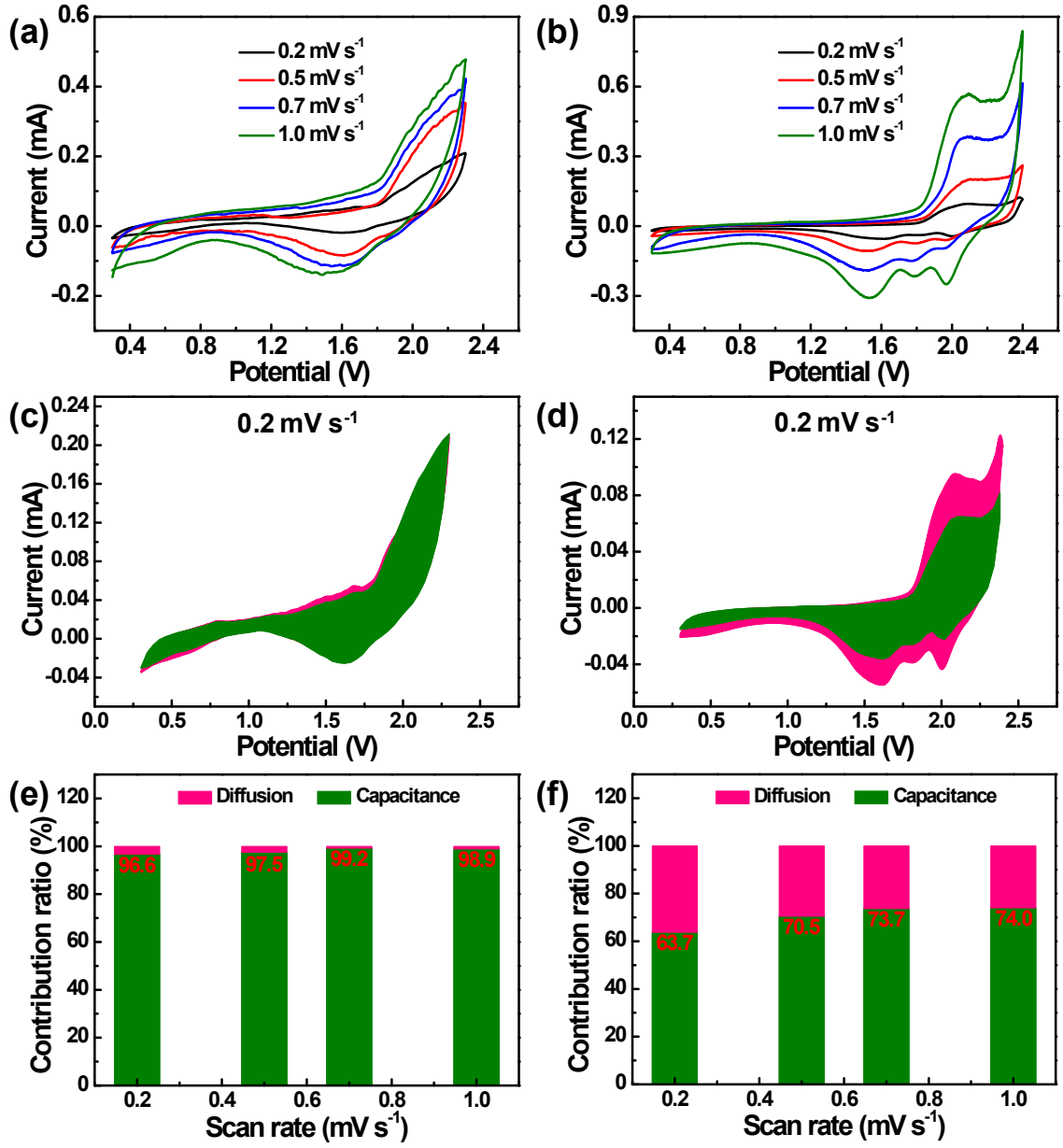

Fig. S12. Kinetic analysis of the AC (a,c,e) and GNF7 (b,d,f) cathodes. CV curves at various scan rates (a,b). Separation of the capacitive and diffusion-controlled contributions at a scan rate of 0.2 mV s^{-1} (c,d). Contribution ratio of the capacitive and diffusion-controlled at different scan rates (e,f).

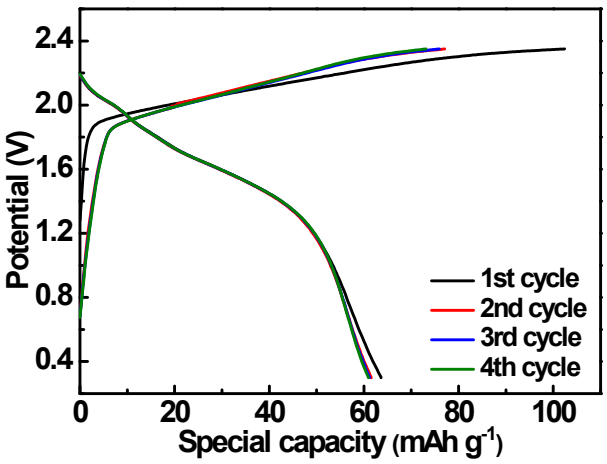

Fig. S13. The charge-discharge curves for the first four cycles of GNF7 cathode at a current density of 200 mA g^{-1}.

Table S1. The calculated I_D/I_G of amorphous carbon before and after cathodic electrolysis under different conditions.

Samples No.	Conditions	D peak position (cm^{-1})	G peak position (cm^{-1})	I_D/I_G
AC	Amorphous Carbon	1309	1571	1.054
GNF1	800 °C-2.6V-2h	1345	1575	0.324
GNF2	800 °C-2.7V-2h	1345	1579	0.236
GNF3	800 °C-2.8V-2h	1351	1581	0.223
GNF4	800 °C-3.0V-2h	1352	1582	0.201
GNF5	850 °C-2.8V-0.5h	1349	1571	0.118
GNF6	850 °C-2.8V-1h	1344	1572	0.117
GNF7	850 °C-2.8V-2h	1356	1583	0.112
GNF8	700 °C-2.7V-2h	1330	1575	0.969
GNF9	700 °C-3.0V-2h	1343	1571	0.579
GNF10	750 °C-3.0V-2h	1337	1573	0.340

Table S2. The calculated graphitization degree of amorphous carbon before and after cathodic electrolysis under different conditions.

Samples No.	Conditions	2θ (°)	d_{002} (Å)	g (%)
AC	Amorphous Carbon	25.219	3.529271	-103.804
GNF1	800 °C-2.6V-2h	25.986	3.426098	16.1651
GNF2	800 °C-2.7V-2h	25.992	3.425321	17.0689
GNF3	800 °C-2.8V-2h	26.008	3.42325	19.477
GNF4	800 °C-3.0V-2h	26.013	3.422603	20.229
GNF5	850 °C-2.8V-0.5h	26.032	3.420148	23.0836
GNF6	850 °C-2.8V-1h	26.112	3.409851	35.0571
GNF7	850 °C-2.8V-2h	26.186	3.40038	46.0669
GNF9	700 °C-3.0V-2h	25.706	3.462778	-26.486
GNF10	750 °C-3.0V-2h	25.78	3.453006	-15.123
GNF11	700 °C-3.0V-5h	26.004	3.423767	18.8753

Table S3. Comparison between this work and the previous reported graphite materials by different synthetic approaches.

Synthetic approaches of graphite	Carbon sources	Assisted by catalysts	Product purity	Temperature (°C)	Energy consumption (kWh kg^{-1})	BET surface area (m^2 g^{-1})	Pore volume (cm^3 g^{-1})	I_D/I_G	d_{002} (Å)	Ref.
Thermal annealing	Only a few graphitizable precursors	None catalysts	High	2200	32.1	---	---	---	3.39	1
				>2500	---	---	---	0.30	3.39	2
				2300	---	260	0.34	---	3.42	3
Microwave heating	Most amorphous carbon precursors	Ni, Fe, Co catalysts	Medium	1170	---	---	---	---	3.43	4
				1418	3.0	---	---	0.30	3.42	5
Chemical vapor deposition	CH_4, C_2H_2, C_2H_4, C_6H_6, CH_4+H_2, etc.	Ni, Fe, Co catalysts	Medium	950	---	---	---	0.66	---	6
				>1000	---	---	---	---	3.35	7
				700	5.5	109	---	1.50	3.41	8
				850		870	0.80	0.62	3.45	9
Catalytic graphitization	Most amorphous carbon precursors	Ni, Fe, Co catalysts	Low	650	---	760	0.67	---	3.40	10
				900	---	275	0.22	---	3.35	11
				1000	12.8	907	0.64	0.40	---	12
Molten-salt electrolysis	All amorphous carbon precursors	None catalysts	High	820	5.5	---	---	0.11	---	13
				>700	4.5	165.7	0.83	0.11	3.40	This work

Table S4. The physical properties of amorphous carbon before and after cathodic electrolysis under different conditions.

Samples No.	Conditions	Specific surface area (m^2 g^{-1})	Pore volume (mm^3 g^{-1})	Pore diameter (Mode Dv(d)) (nm)	Average pore diameter (nm)
AC	Amorphous Carbon	108.00	349.40	2.45	17.00
GNF7	850 ^{o}C-2.8V-2h	165.70	825.80	2.46	39.17

References

1 K. Kawamura and R. Bragg, *Carbon*, 1986, **24**, 301-309.

2 M. Endo, Y. A. Kim, T. Hayashi, T. Yanagisawa, H. Muramatsu, M. Ezaka, H. Terrones, M. Terrones and M. S. Dresselhaus, *Carbon*, 2003, **41**, 1941-1947.

3 A. B. Fuertes and S. Alvarez, *Carbon*, 2004, **42**, 3049-3055.

4 K. S. Yang, Y. J. Yoon, M. S. Lee, W. J. Lee and J. H. Kim, *Carbon*, 2002, **40**, 897-903.

5 T. Kim, J. Lee and K.-H. Lee, *RSC Adv*., 2016, **6**, 24667-24674.

6 A. N. Obraztsov, E. A. Obraztsova, A. V. Tyurnina and A. A. Zolotukhin, *Carbon*, 2007, **45**, 2017-2021.

7 W. Cai, R. D. Piner, Y. Zhu, X. Li, Z. Tan, H. C. Floresca, C. Yang, L. Lu, M. J. Kim and R. S. Ruoff, *Nano Res.*, 2009, **2**, 851-856.

8 D. Hulicova-Jurcakova, X. Li, Z. Zhu, R. de Marco and G. Q. Lu, *Energy Fuels*, 2008, **22**, 4139-4145.

9 R. Atchudan, S. Perumal, T. N. J. I. Edison and Y. R. Lee, *RSC Adv.*, 2015, **5**, 933643-93373.

10 M. Sevilla and A. B. Fuertes, *Carbon*, 2006, **44**, 468-474.

11 D. Zhai, H. Du, B. Li, Y. Zhu and F. Kang, *Carbon*, 2011, **49**, 718-736.

12 Y. Liu, Q. Liu, J. Gu, D. Kang, F. Zhou, W. Zhang, Y. Wu and D. Zhang, *Carbon*, 2013, **64**, 132-140.

13 J. Peng, N. Chen, R. He, Z. Wang, S. Dai and X. Jin, *Angew. Chem. Int. Ed.*, 2017, **129**, 1777-1781.